Surface CO_2 emission and rising bubble plumes from degassing of crater lakes in São Miguel Island, Azores

GLADYS MELIÁN[1,2,3*], LUÍS SOMOZA[4], ELEAZAR PADRÓN[1,2,3], NEMESIO M. PÉREZ[1,2,3], PEDRO A. HERNÁNDEZ[1,2,3], HIROCHIKA SUMINO[5], VICTOR H. FORJAZ[6] & ZILDA FRANÇA[6]

[1] Environmental Research Division, Institute of Technology and Renewable Energies (ITER), 38611 Granadilla de Abona, Tenerife, Canary Islands, Spain.
[2] Instituto Volcanológico de Canarias (INVOLCAN), 38400 Puerto de la Cruz, Tenerife, Canary Islands, Spain.
[3] Agencia Insular de la Energía de Tenerife (AIET), 38611 Granadilla de Abona, Tenerife, Canary Islands, Spain
[4] Marine Geological Resources Division, Geological Survey of Spain (IGME), Rios Rosas 23, Madrid, Spain.
[5] Geochemical Research Center, Graduate School of Science, The University of Tokyo, Hongo, Bunkyo-Ku 113-0033, Tokyo, Japan.
[6] Observatório Vulcanológico e Geotérmico dos Açores (OVGA), Açores, Portugal.

Submitted to

VolLakes Special Publication book

March, 2015

*Correspondence author, present address: Environmental Research Division, Instituto Tecnológico y de Energías Renovables (ITER), 38611 Granadilla, S/C de Tenerife, Spain. Tel: (34)-922-747700; Fax: (34)-922-747701, E-mail: gladys@iter.es

Abstract

We report in this paper the first detailed study on the types and distribution of active subaqueous fumaroles and surface diffuse CO_2 degassing, performed in the three main volcanic lakes of São Miguel Island (Sete Cidades, Fogo and Furnas), Azores archipelago, Portugal. The results of the surveys, carried out in May 2011 using a floating accumulation chamber and a dual beam 50 and 200 kHz echo sounder, revealed a very low surface CO_2 degassing at the three lakes, in the range 32-608 kg d^{-1}, but dense subaqueous degassing plumes located in the north of Furnas (7.5-9 plumes/100 m^2), with moderate density degassing in Fogo (1.5-2 plumes/100 m^2) and Sete Cidades crater lakes (1-1.5 plumes/100 m^2). The echo sounder detected hydro acoustic signatures interpreted as acoustic flares, "puffing" bubble plumes or walls of bubbles associated with numerous subaqueous fumaroles. The recorded echograms show the bubbles rise at speeds averaging between 19–30 cm/s at the bottom with frequencies of release from 1-2 to 31 s. Most subaqueous fumaroles are faded out by dissolution of CO_2 before reaching the lake surface. Dissolution processes are enhanced by the pH range observed in the three volcanic lakes (~7-9). Observed dissolved CO_2 values indicate that the pressure of this gas in the three lakes remained much lower than the hydrostatic pressure and the risk of alimnic eruption is negligible. We suggest that the rising levels of CO_2 sourced from the subaqueous bubbles could constitute a critical fuel for sub-surficial phytoplankton layers interpreted as horizontal acoustic plumes beneath the lake surface. The highest density of subaqueous degassing bubbling correlates with recent submerged secondary craters formed around the caldera rims of the three Late Quaternary stratovolcano complexes of São Miguel Island. Our results emphasize the need to perform regular surface degassing studies as an important volcanic surveillance tool in the Azores archipelago.

Key words: Diffuse degassing, echo-sounding, Sete Cidades, Furnas, Fogo, Azores, CO_2.

1. Introduction

Most of the world's lakes are net sources of CO_2 to the atmosphere (Cole et al., 1994). This process is much more evident in the volcanic lakes, because they are major sites of emissions and condensation for volatile elements produced by magmatic activity. Recent estimates of global CO_2 emissions from volcanic lakes (~117 Mt/yr) show a similar value to recent estimated emissions for submarine and is equivalent to 30% of the global degassing of subaerial volcanism (Pérez et al., 2011). The main hazard in volcanic lakes is the accumulation of magmatic CO_2 that may result in the sudden release of enormous amounts of dissolved CO_2 gas trapped at the bottom of lakes. This process is well known by the scientific community after the Lake Monoun (1984) and Lake Nyos (1986) disasters, both in Cameroon (Sigurdsson et al., 1987; Le Guern and Sigvaldason, 1989; Kling et al., 2005; Kusakabe et al., 2008). Degassing at volcanic lakes occurs by an advective mechanism, in the form of ascending bubbles from active subaqueous fumaroles, and by molecular diffusion through the water-air interface. The latter is called diffuse degassing, and represents an important amount of the total CO_2 emission from volcanic lakes (Pérez et al., 2011). The magnitude of the diffuse CO_2 through the air-water interface depends on the concentration gradient between the air and the surface water.

Echo sounding methods have mainly been used on volcanic lakes for bathymetric purposes in Kawah Ijen Crater Lake, East Java, Indonesia, for example (Takano et al., 2004) or to map underwater volcanic structures in the Yellowstone Lake (Morgan et al., 2003). Due to the high contrast of acoustic impedance between water and the free gas phase, subaqueous fumaroles strongly scatter the acoustic energy in water (Greinert et

al., 2010). Echo sounding techniques also provided useful information on degassing rates and the carbon dioxide dynamics of the Kelud volcanic lake (Caudron et al. 2012). The Azores archipelago has 88 shallow lakes, most of which are associated with craters or subsidence calderas. This work presents the first results of diffuse CO_2 degassing and echo sounding surveys carried out in May 2011 at Furnas, Fogo and Sete Cidades volcanic lakes. These are the main volcanic craters of São Miguel Island, located in calderas of major stratovolcanoes where pre-historical and historical eruptions (between 1439-44 AD and 1630 AD) have occurred. The main goals of this work are: 1) to study the spatial distribution of diffuse CO_2 degassing; 2) to estimate the total output of CO_2 emitted into the atmosphere; 3) to analyze the types and distribution of active subaqueous fumaroles identified by means of a dual beam 50 and 200 kHz echo sounder; and 4) to study the possible CO_2 accumulation in the deep water in three main volcanic crater lakes of the São Miguel Island (Azores archipelago).

2. Geological background

Azores archipelago consists of nine volcanic islands, situated in the North Atlantic Ocean about 1,360 km west of continental Portugal. The geological setting of the Azores region is dominated by the role of the American, Eurasian and African lithospheric plate boundaries (Miranda et al., 2014). The most important tectonic structures recognized in the area are the Mid-Atlantic Ridge and the Terceira Rift. Together they are the main source of the seismic and volcanic activity recorded in the region (Lourenço et al., 1998). São Miguel (Fig. 1) is the largest and most populated island of the Azores archipelago and is located in the eastern part of the Terceira Rift. The island is formed by several volcanic edifices situated along a general E-W trend and is crossed by NW-SE, NE-SW, WNW-ESE and E-W regional tectonic structures (Trota, 1998). The recent volcanism of the São Miguel Island is related to three main volcanic

centers: Sete Cidades, Fogo and Furnas (Forjaz, 1984; Moore, 1991). During the last 5,000 years, the activity of these volcanic centers has resulted in at least 57 eruptive processes, with five eruptions during the past 500 years (Moore, 1991).

Volcano-hydrothermal fluid discharges in São Miguel are evident by the existence of low temperature fumaroles (95–100ºC), steaming ground, thermal springs, cold CO_2-rich springs and areas of soil diffuse degassing (Viveiros et al., 2010). There are several thermal water discharges and cold-CO_2 enriched springs on São Miguel Island that discharge mainly from perched-water bodies and with a clear mantle CO_2 signature (Cruz & França, 2006).

The Sete Cidades volcano (350 m.a.s.l) is composed of a semi-circular crater slightly elongated along a NW-SE direction (5.2 x 4.8 km) with a total area of 18.5 km^2. Within the Sete Cidade crater, two separated crater lakes are aligned from SSW to NNE: the Lagoa Azul (Blue Lake) to the north and the Lagoa Verde (Green Lake) to the south (Fig. 1). The Lagoa Azul lake is slightly elongate along the NW direction (2.7 x 2.1 km) covering a total extension of 3.6 km^2. The Lagoa Verde is also an elongate lake (5.2 x 4.8 km) covering a total extension of 0.7 km^2. In this way, the two crater lakes cover around 25% of the Sete Cidades volcano crater. The caldera of Sete Cidades volcano formed approximately 22,000 years ago after the eruption of several cubic kilometers of trachyte pumice. Six vents are present on the floor of Sete Cidades caldera in a roughly circular pattern. Other vents may be submerged beneath Lagoa Azul and Lagoa Verde. The youngest Sete Cidades intra-caldera eruption formed the Caldeira Seca pumice ring. It has a radiocarbon age of 500±100 years B.P. (Shotton & Williams, 1971) and correlates with a reported eruption at the time of Portuguese discovery of the island in the middle of the fifteenth century. Only two warm springs are known, near Mosteiros

on the northwestern coast and at Ponta da Ferraria on the western coast (Fig. 1). The latter has a temperature of about 50°C (Moore, 1991).

Furnas volcano, a stratovolcano about 800 m a.s.l, occupies the east-central part of São Miguel. The Furnas crater lake is located within the Furnas caldera, the third major volcano of the São Miguel Island (Fig. 1). It is an elongate lake (2.0 x 1.5 km) covering a total extension of 1.9 km^2. The geographical distribution of the water types in Furnas caldera reveals a WSW–ENE lineament of volcanic CO_2 flux (Cruz et al., 1999). Furnas volcano releases much more CO_2 in a non-visible or diffuse way (1,100 t d^{-1}; Viveiros et al., 2010), than that released by water springs (4,556 t y^{-1}; Cruz et al., 1999), without taking into account the contributions from fumaroles, bubbling pools, cold CO_2-rich springs or Furnas lake. The Lagoa das Furnas is located at the western side of the inner crater. During the last 5,000 years, at least 17 trachytic eruptions have taken placeat Furnas volcano, including 10 eruptions within the inner caldera that formed a trachyte and pumice dome (Moore, 1991). Hot springs are prominent at Furnas volcano, the distribution of which is shown by Zbyszewski et al. (1958). Those on the northern shore of Lagoa das Furnas are probably related to the nearby caldera-bounding fault. Hot springs in the village of Furnas are probably associated with the Furnas crater or with radial fractures that formed during emplacement of the trachyte domes (Booth et al., 1978).

The Lagoa do Fogo (“Fire Lake”) is a crater lake located in the inner part of the Agua de Pau volcano, a stratovolcano with a prominent 3.0 x 2.5 km caldera with a total area of 7.5 km^2 and walls as highs as 300 m (Fig. 1). At least five eruptions of trachyte pumice have occurred from vents mostly within the inner caldera during the past 5,000 years (Booth et al., 1978). There have been two recent eruptions reported close to the Lagoa do Fogo (Moore, 1990). The A.D. 1563 eruption formed low spatter ramparts on

153 top of Queimado, a relatively old trachyte dome about 6 km west-northwest of Lagoa do
154 Fogo (Moore, 1990). In A.D. 1652, a strombolian eruption built a cinder cone and
155 extruded flows about 10 km west of Lagoa do Fogo (Weston, 1964). Several hot
156 springs, with temperatures commonly near boiling, are located on Agua de Pau, mainly
157 on its northwestern flank (Zbyszewski et al., 1958). The hot springs suggest that hot
158 rock or magma associated with the late Pleistocene and Holocene eruptions is close to
159 the surface (Moore, 1991). Fogo volcano has developed an active geothermal system
160 that is currently being exploited on its northern flank to produce over 100 GWh of
161 electricity generated by geothermal power plants (Wallenstein et al., 2007).

162 **3. Methods, analyzing and data processing**

163 During May 2011, surface diffuse CO_2 efflux and echo sounder surveys were performed
164 at Furnas, Fogo and Sete Cidades volcanic lakes, São Miguel Island. Diffuse CO_2
165 emission was measured in 102, 80 and 167 sampling sites selected at Furnas, Fogo and
166 Sete Cidades, respectively to obtain an almost homogeneous pattern distribution,
167 following the accumulation chamber method (Parkinson, 1981), with the chamber
168 placed on a flotation device (Huttunen et al., 2003; Pérez et al., 2011). At each sampling
169 site, pH, temperature and conductivity were measured at 15 cm depth from the water
170 surface, by means of an Oakton pH/CON 300 meter. Spatial distribution maps were
171 constructed using sequential Gaussian simulation (sGs) provided by the *sgsim* program
172 (Deutsch & Journel 1998; Cardellini et al., 2003). The final maps were constructed as
173 an average of 100 equi-probable realizations performed over a grid of 11,358, 4,836 and
174 3,967 squared cells (20m×20m) for Sete Cidades, Furnas and Fogo lakes, respectively,
175 following spherical variogram models that honor the experimental variograms.

176 The echo sounder (ES) surveys were carried out by means of a Lowrance HDS-5
177 equipped with a dual frequency (50 and 200 kHz) transducer. Boat speeds range on

178 average between 0.5 and 3 knots. Digital data of the ES were processed by means of the
179 Sonar Viewer 2.1.2 software. Extracted bathymetric data were converted from the
180 Lowrance-type Mercator projection to Universal Transverse Mercator using ArcGIS
181 10.2. The bathymetric grid and 3D models of the crater lakes were generated using
182 Fledermaus IVS software. We used mainly the 50 kHz sampling frequency for the
183 analysis of the data, because data analyzed at 200 kHz missed bubbles that were
184 detected at 50 kHz, as demonstrated in Caudron et al. (2012). The calculating density
185 map of the acoustic plumes was constructed using the Kernel density procedure with
186 ArcGIS 10.2. This procedure calculates the number of plumes per unit of area from
187 using a kernel function to fit a smoothly tapered surface to each grid cell (i.e. 10 m).
188 Thus density of acoustic plumes is defined as the number of plumes per unit of area
189 (e.g. 150/km^2 or 1.5/100 m^2).
190 To study the possible water stratification and CO_2 accumulation in the three volcanic
191 lakes, five vertical profiles of dissolved gas sampling were carried out (2 in Furnas, 1 in
192 Fogo and 2 in Sete Cidades). The vertical profiles were completed at the deepest point,
193 located after a short echo sounding survey. A 2.2 liters WaterMark horizontal PVC
194 water bottle was used to collect water samples at different depths. For each water
195 sample, chemical analyses were carried out in the laboratory. Cl^- and SO_4^{2-} were
196 analyzed by means of a Dionex DX-500 ion-chromatograph and HCO_3^- (main carbon
197 specie) was performed by automatic titration with a Metrohm 716 DMS Titrino. The
198 accuracy of the analysis was estimated at ~2-3 %. Dissolved He, N_2, $CO_{2(aq)}$ and O_2
199 were analyzed following the method of Capasso & Inguaggiato (1998), with pure Ne as
200 host gas and a quadrupole mass spectrometer (QMS) Pfeiffer Omnistar 422. The
201 detection limit for He was estimated to be about 0.05 ppmV, while analytical accuracy
202 was approx. 2.5 % and 5 % for the main gas components and minor gas compounds,

203 respectively. Additionally, at the deepest point of each profile, isotopic composition of
204 dissolved helium was also analyzed. Dissolved gases in these samples were extracted as
205 explained by Padrón et al. (2013) and analyzed to determine helium and neon
206 concentrations and helium isotopic ratios following the method of Sumino et al. (2001).
207 Results are expressed as times R_A, being R_A the atmospheric $^3He/^4He$ ratio (R_A=1.384 ×
208 10^{-6}, Clarke et al., 1976).

209 **4. Results and discussion**

210 **4.1 Sete Cidades crater lakes**

211 **4.1.1 Spatial distributions**

212 Figure 2 depicts the spatial distribution of diffuse CO_2 emission (A), water pH (B) and
213 temperature (C) values. Low diffuse CO_2 efflux values were measured at the water
214 surface of Sete Cidades, ranging between non-detected values (<0.5 g m^{-2} d^{-1}, 66 % of
215 the data) and 4.1 g m^{-2} d^{-1}. The highest values were measured mainly in the NW coastal
216 areas of the Lagoa Azul (Fig. 2A). The diffuse CO_2 emission, computed to 608 ± 74 kg
217 d^{-1} released over an area of 4.5 km^2, represent one of the lowest normalized CO_2
218 emission rates (135 kg km^{-2} d^{-1}) reported to date for a volcanic lake (Pérez et al., 2011).
219 Surface water pH ranged in slightly basic values, between 7.1 and 9.1, with an average
220 value of 8.1. A slight acidification (pH~7.6) can be observed in the water surface in the
221 NW coastal area of Lagoa Azul, which suggests a relatively good spatial correlation
222 between CO_2 emission and pH (Fig. 2B). In the case of water temperature, it ranged
223 between 13.3 and 15.9ºC, with an average value of 15.1ºC, while air temperature was
224 ~17ºC. Warmer waters (>15ºC) were observed in the middle of Lagoa Azul (Fig. 2C).
225 Water conductivity showed an almost constant value around 113 μS/cm, without any
226 significant spatial variability with a relative standard deviation (RSD) of 0.4%.

227 **4.1.2 Vertical profiles**

228 Two profiles were performed in Sete Cidades crater lake, one in Lagoa Azul and the
229 other in Lagoa Verde, reaching 21 and 19 m depth, respectively (white star in Fig. 2).
230 Both profiles showed a similar descending trend in the pH value from ~9 to ~7 (Fig.
231 3A), which indicates that dissolved CO_2 is mainly present as HCO_3^- and $CO_{2(aq)}$. Since
232 the upper water layers in both profiles showed the most basic values (~9),
233 eutrophication processes cannot be excluded. The descending trend in the pH is likely
234 due to dissolution of CO_2 that is being released from the bottom of the lake. This
235 process is more evident in Lagoa Azul. Figures 3B and 3F do not show any significant
236 trend neither in the amount of HCO_3^- nor in the total CO_2 dissolved in both Lagoa
237 Verde and Azul. Bicarbonate values ranged between 30.6 and 39.3 mg/L (Fig. 3B).
238 Total dissolved CO_2 (anionic CO_2 as HCO_3^- plus $CO_{2(aq)}$) ranged between 36 to 53 mg/L
239 (Fig. 3F). Slightly lower total dissolved CO_2 values (~20-30 mg/L) were reported by
240 Cruz et al. (2006). However, there is no record of any increase in the CO_2 degassing rate
241 over the period 2003-2011.
242 At the sites where the vertical profiles were performed, water temperature descended
243 gradually with depth from ~16ºC at the surface to ~13ºC at the bottom for Lagoa Verde
244 and the ~16ºC at the surface to ~15ºC at the bottom for Lagoa Azul (Fig. 3C), which
245 indicates the existence of a dense stratification and rules out the possible existence of
246 hot springs at depth at the sites where the profiles were made. A thermocline was not
247 present in Sete Cidades lake. The deepest waters of higher ratios N_2/O_2 (higher than
248 N_2/O_2 ratio in air-saturated water, ASW) were measured at the bottom of both Lagoa
249 Verde and Azul, suggesting an addition of endogenous or biogenic nitrogen (e.g.
250 benthic nitrogen production).

The $^{3}He/^{4}He$ ratio analyzed in the water of Lagoa Azul at 21 m depth (deepest point) showed a value similar to the atmospheric one, 0.95 ± 0.04 R_A, while in Lagoa Verde (19 m depth), the result was 0.67 ± 0.04 R_A.

4.1.3 Echo sounding results

4.1.3.1 Lagoa Azul crater lake

Figure 4A show the morphology of Sete Cidades crater lake. The bottom lake morphology of the Lagoa Azul is split into two different parts (Fig. 4B). The southern part is composed by a small circular depression, 450 m in diameter and 6 meter water depth (mwd), with flank slopes ranging between 3 and 4º. The northern part is composed by a stepped platform ranging from 5 to 22 mwd that ends in the north with a flat basin with 23-24 mwd (Fig. 4B). The platform and the deep basin are connected by an 8-9º steep slope. The deepest basin of the Lagoa Azul reaching 25 mwd is located close to the northern limit of the main crater of the Sete Cidades volcanic system (Figs. 1 and 4B).

Features of bubbles in echograms

The locations of the observed bubble plumes in the bottom of the lake are indicated as red dots in Figures 4, 5A and 5B. Most of the bubble plumes identified in the Lagoa Azul crater lake are located within the deep basin and along the steeped slope that connects the shallow platform (Fig. 4B). Except for the shallow parts, the north of Lagoa Azul exhibits frequent vertical plumes of bubbles (Figs. 5A and 5B). The bottom of the deep basin shows very concentrated zones that we termed as walls of bubbles (Fig. 5C). These walls or clouds sourced from the bottom lake form columns that span 190-225 m wide (Fig. 5C). The clouds that are only observed on the 50 kHz echogram are constituted by medium scattering values with numerous high backscattering small hyperbolas within the clouds when they are zoomed. High scattering crescent shapes

observed between the walls of bubbles are possibly related to a reduction of the speed of the boat from 3 to 0.5 knots expanding the shape of the targets and forming crescents. Most of the high density walls are sourced from the flanks of the steep slopes (Fig. 5C), reflecting possibly that active diffuse degassing is related to fault structures within the crater lake. A horizontal and strongly stratified 2-3 m thick layer showing very high backscatter values is extended over the subsurface of the deep basin of the Lagoa Azul at water depths ranging between 0.5 and 3 m (Fig. 5C).

Towards the border of the deep basin of the Lagoa Azul, the hydroacoustic manifestations of bubbling are identified as continuous streams of bubbles (e.g. Fig. 6A) and intermittent bursts of bubbles (e.g. Figs. 6B and 6C). The 50 kHz echograms of these bubble plumes illustrate the intermittency of the degassing process or puffing (Figs. 6B and 6C). Another characteristic of these bubble plumes is that they are also observed in the 200 kHz echogram as thinner plumes. Normally, data at 200 kHz miss bubbles that are detected at 50 kHz. The detection of these plumes by higher frequencies (with shorter wavelengths), reducing the range for observing targets, might indicate that they are formed by bubbles with greater diameters (Caudron et al., 2012).

Density and distribution of plumes

The density of plumes identified at Lagoa Azul show the maximum are located in the north of the lake (Fig. 5A). The calculated density of plumes reaches its highest values of 150 plumes/km^2 in the deepest basin of Lagoa Azul (Fig. 5B). The lake floor area of Lagoa Azul affected by bubbling plumes has an extension of 2.4 km^2 (Fig. 5B). This area with high density of bubbling plumes coincides with a certain rise in the lake surface water temperature up to 16ºC.

4.1.3.2 Lagoa Verde crater lake

300 The morphology of the Lagoa Verde (Fig. 4C) is constructed of an asymmetric elongate
301 (1.2 x 0.78 km) deep basin with the bottom located at 18-21 mwd at its southern side.
302 The western flank of this basin is constructed of a stepped platform with water depths
303 ranging from 4 to 18 m. In contrast, the eastern flank of the deep basin does not show
304 such stepped morphology. The maximum slope of this crater lake averages 3-4º on the
305 eastern flank of the deep basin. In this way, the bubble plumes identified in the Lagoa
306 Verde are located along the deep basin and on the steep eastern flank of this basin (Fig.
307 5B).
308 *Features of bubbles in echograms*
309 The hydroacoustic manifestations of degassing in the Lagoa Verde crater lake are
310 mainly constituted by bursts of bubbles and isolated flares (Fig. 5D). The bursts of
311 bubbles are similar to those observed in the Lagoa Azul. These are composed of
312 ascending trains of bubble plumes with their tops at approximately at 10, 7 and 6 mwd
313 (Fig. 6D). These bubble plumes are sourced from 12 mwd and disappear at 6 mwd,
314 indicating a rapid process of bubble dissolution in the water column. This process gives
315 rise to high backscatter “walls” above the bubble plumes and beneath the subsurface
316 horizontal layer. At these sites of degassing, the horizontal layer is thickened and
317 “bright” very high backscatter spots are identified along the horizontal layer at the
318 intersection with the disappearing rising bubble plumes (Fig. 6D). Isolated vertical
319 plumes are also identified as acoustic columns that link the bottom of the lake to the
320 horizontal layer (Fig. 5D). In contrast to bubble plumes, flares show slightly downward
321 tapering cone shapes separated by 20 m width and 11-12 m height. One of observed
322 difference between the burst of bubbles and isolated flares are that the latter are sourced
323 from depressions of the lake bottom, indicating a sourceof diffuse and focused
324 degassing respectively.

Density and distribution of plumes

The calculated density of plumes ranges between 125 and 150 plumes/km^2 with their maximum in the deepest basin of Lagoa Verde (Figs. 5B). The total area of lake floor of the Lagoa Verde affected by bubbling acoustic plumes is estimated to be 0.9 km^2 (Fig.5B). As occurred in the Lagoa Azul, the pattern of the density maps point to degassing mostly throughout peripheral secondary craters within the main caldera complex (Fig.5B). A third zone of moderate rate degassing (ranging between 50-75 plumes/km^2) is located between the two lakes. This could be related to a small crater within the Sete Cidades caldera at the intersection with the NW-SE Mosteiro Graben (Figs. 1 and 5B). This is a pronounced structure on the northwestern flank of the caldera interpreted to be the sub-aerial segment of the Terceira Rift (Queiroz and Gaspar, 1998).

4.2 Furnas crater lake

4.2.1 Spatial distributions

Figure 7 depicts the spatial distribution of diffuse CO_2 emission values (A), water pH (B) and temperature (C). Similarly as was observed in Sete Cidades, low diffuse CO_2 effluxes values were measured at the water surface of Furnas, ranging between non-detected values (<0.5 g m^{-2} d^{-1}, 82% of the data) and 13.9 g m^{-2} d^{-1}. Although diffuse CO_2 effluxes were low, two considerable degassing sites can be identified (Fig. 7A): the shoreline near the Caldeira das Furnas hot springs, that occurs in the Furnas lake fumarolic field, with temperatures approaching boiling point of the gas-rich water at surface conditions (Cruz et al., 1999), and a site located slightly north of the center of the lake. Both sites were also characterized by the lowest surface pH values (Fig. 7B). Furnas lake fumarolic field is an anomalous diffuse CO_2 degassing structure with CO_2 emission values of more than 7 kg m^{-2} d^{-1} (Vivieros et al., 2010). The highest diffuse CO_2 emission values measured in the north of the lake are spatially correlated with this

diffuse CO_2 degassing structure. The diffuse CO_2 emission was estimated at 32 ± 11 kg d^{-1} released by a surface of 1.9 km^2, which represents a lower normalized CO_2 emission rate (17 kg km^{-2} d^{-1}) than that measured in Sete Cidades in this work. In the case of water temperature, it ranged between 13.9 and 15.6ºC, with an average value of 14.9ºC, while air temperature was ~17ºC. No significant changes in surface water temperature were observed in Furnas Crater Lake (Fig. 7C). Spatial distribution of water conductivity is not shown because the values did not show any significant spatial variability, with an almost constant value of ~150 μS/cm with a RSD of 1.3%.

4.2.2 Vertical profiles

Two profiles were performed in Furnas crater lake, S-profile in the deepest part (pink star in Fig. 7) and N-profile close to the shoreline near the Caldeira das Furnas hot springs (white start in Fig. 7), reaching 9 and 5 m depth, respectively. No significant trend was observed in the pH of the waters (Fig. 3G). Water temperature data in both profiles indicate that the lake was not appreciably stratified during the study. The S-profile temperature values decreased with depth from ~15.6ºC at the surface to 14.6ºC at the bottom (Fig. 3I). This behavior was not present in the N-profile, where the water temperature showed an almost constant value around 15ºC (Fig. 3I). The increase in the HCO_3^- concentration with depth is more evident in the N-profile, where the higher CO_2 degassing rates were measured (Fig. 3H). Total dissolved CO_2 ranged between 40 to 58 mg/L (Fig. 3F). Cruz et al. (2006), reported an almost constant dissolved CO_2 value ~40 mg/L.

SO_4^{2-} and Cl^- concentrations were studied only in the S-profile. Although the concentrations of these anions were almost constant (Figs. 3J and 3K) throughout the profile, they reached the higher values at the bottom of the lake. Furnas showed the highest N_2/O_2 ratios in the deepest waters, suggesting an addition of endogenous or

biogenic benthic nitrogen production. The deepest waters of Furnas showed also discrete enrichments in He (Fig. 3L). Assuming that helium concentrations in Furnas Lake can be described by the concentration profiles observed (Fig. 3L), it is possible to estimate the helium emissions through the water surface of Furnas by applying a pure diffusive model. According to Fick's law, the gas flux in the water surface is driven by the concentration gradients along the depth and the diffusivity of the gas in water:

$$F_i = -D_{i(w)} \frac{\partial C_{i(w)}}{\partial z}$$

being F_i the flux of i (kg m^{-2} s^{-1}), $D_{i(w)}$ the diffusion coefficient in water (m^2 s^{-1}), $C_{i(w)}$ the concentration of i in water (kg m^{-3}) and z the depth (m). In the case of helium, we used $D_{He(w)}$ at the average temperature of Furnas Lake waters (15ºC), that is ~5.45 x 10^{-9} m^2 s^{-1}. $D_{He(w)}$ was calculated as an interpolation of the values between 10º and 20ºC reported by Verhallen et al. (1984). The observed concentrations of helium at different depths in both N- and S-profiles, were fitted with the following exponential decay function:

$$[He]_w = 1.58\ x\ 10^{-8} e^{-(\frac{z}{1.9})} + 4.13\ 10^{-7}$$

$$[He]_w = 1.02\ x\ 10^{-7} e^{-(\frac{z}{4.7})} + 5.45\ 10^{-8}$$

for N- and S-profile, respectively. These fitting equations describe the helium concentration (mg/L) in the water as a function of the depth (z). The derivative with respect to depth at a z=0 (water surface) allows for the estimation of helium emissions through the water surface (1.92 km^2) to be in the range of 8 to 20 mg d^{-1}, with a normalized emission value versus the area of 4.2-10.4 mg km^{-2} d^{-1}. The ^{3}He/^{4}He ratio analyzed at 9 m depth (S-profile) was 1.12 ± 0.04 R_A.

4.2.3 Echo sounding results

The maximum depth of the Furnas crater lake is 12 m located at its center (Fig. 8A). The slope of the lake flanks range from 9 to 12º whereas at its center the deepest basin shows slopes lower than 0.2º.

Features of bubbles in echograms

Subaqueous bubbling in the Furnas lake are identified as hydroacoustic `plumes´ in the water column; i.e. strong backscatter signals 8-10 m height with a flare-like shape which are rooted to the lake floor (Figs. 8B and 9). Flares are mainly observed on the slope of the northern flank of the lake at water depths ranging between 5 and 12 m and are located close to the field of subaerial hot springs called Caldeiras das Furnas (Fig. 8A). Normally these flares ranging between 5 and 10 m in height reach the uppermost horizontal layer of high backscatter located at between 3 and 0.5 mwd (Fig. 8B). Most of the flares are sourced from the floor of the lake forming depressions or holes. (Fig. 8B), which show the same morphology as the nearby subaerial hot springs termed as "Caldeiras das Furnas" (Fig. 8B). The subaqueous "furnas" are characterized by 1-3 m deep 40-50 m wide lake floor depressions that are partially filled by recent sediments (Fig. 8B).

Density and distribution of plumes

Flares are mainly concentrated on the north basin of the Furnas crater lake around the area where the hot springs termed as the "Caldeiras da Furnas" are found (Fig. 8A). The density map shows the highest values of 750-900 plumes/km^2 in this area (Figs. 9A). However, the lake floor affected by this high density of plumes is only of 0.1 km^2. Other areas with moderate density ranging 350-400 plumes/km^2 are also observed in the center of the Furnas crater lake (Fig. 9A). Figure 9B shows 3D imaging of the flares rising from the bottom of the Furnas crater lake in the profiles C1 and C2 identified in

Figure 9A. At regional scale, the main density of flares identified at Furnas crater lake is located along the border of the caldera rim of the stratovolcanic complex.

4.3 Fogo crater lake

4.3.1 Spatial distributions

Figure 10 shows the spatial distribution of diffuse CO_2 emission values (A), water pH (B) and temperature (C) at the water surface of Fogo Lake. Low diffuse CO_2 effluxes are also shown, ranging between non-detected values (<0.5 g m^{-2} d^{-1}, 63% of the data) and 3.8 g m^{-2} d^{-1}. Highest values of diffuse CO_2 emission (>2 g m^{-2} d^{-1}) were located in the south-east of the lake (Fig. 10A). Furthermore, the spatial variability of surface water pH and temperature was also very low: i.e. water pH and temperature fluctuated within the ranges of 7.0-7.3 and 12.4-12.9ºC, respectively. For this reason, a different color scale was used for their spatial distribution (Figure 10B and 10C) with respect to that used for Sete Cidades and Furnas lakes. The highest CO_2 emission (~4 g m^{-2} d^{-1}) located in the south-east of the lake agreed with water temperature values (~13ºC). This is the reason why this locality was selected for the vertical profile (white star in Figure 10). The diffuse CO_2 emission was estimated at 161 ± 14 kg d^{-1} released over an area of 1.59 km^2, which represents a normalized CO_2 emission rate of 101 kg km^{-2} d^{-1}. Again, we do not show the spatial distribution of water conductivity due to the absence of considerable spatial variability, with an almost constant value of ~42 μS/cm with a RSD of 1.0%.

4.3.2 Vertical profiles

The profile performed in the south-east of Fogo crater lake reached 26 mwd (white star in Fig. 10). No significant trends were observed in any of the parameters analyzed in the profile (Figs. 3M-3R). Total dissolved CO_2 values were the lowest of the three volcanic lakes studied in this work, and ranged between 7 and 8 mg/L (Fig. 3E), similar to values

447 reported by Cruz et al. (2006). No evidence of accumulation of CO_2 at the bottom of the
448 lake was observed. It is worth noting that, although there were no vertical trends that
449 allowed for the application of a diffusion model to estimate the emission of helium,
450 important concentrations of this gas (up to 0.4 cm^3 STP/L) were measured at different
451 depths (Fig. 3R). The $^3He/^4He$ ratio analyzed at 20 m depth was 0.84 ± 0.03 R_A.

452 **4.3.3 Echo sounding**

453 *Features of bubbles in echograms*

454 Two main types of hydroacoustic features related to bubbling have been identified in
455 the Fogo crater lake (Fig. 11A): (i) scattered acoustic hyperbolas staggered up through
456 the water column from the bottom of the lake and (ii) strong backscatter signal columns
457 in the water column rooted to the lake floor. Two large hydroacoustic plumes have been
458 identified in the southern basin of the Fogo crater lake (Fig 11B). These plumes are
459 characterized by very high backscatter values forming 10 m high columns in the water
460 column which are rooted to the lake floor and rise up 3 m below the lake surface (Fig.
461 11B). Both hydroacoustic plumes are connected throughout a strong backscatter
462 horizontal signal 1-2 m below the surface of the lake.

463 *Density and distribution of plumes*

464 The map of density of acoustic anomalies of the Fogo lake show the highest spot of
465 plumes with densities of 150-200/km^2, located in the north part of the Fogo crater lake
466 (Fig. 11C). This high density bubbling spot covers a small zone of 0.158 km^2. At the
467 same time, a zone of moderate plume density (averaging 75-100/ km^2) is also identified
468 at the central and deepest part of the lake at water depths from 12 to 28 meters (Fig.
469 11C). In this sense, the map of density of plumes show a certain NW-SE trend which
470 suggest they could be related to degasification along faults with this orientation (Fig.
471 11C). The location of the two bubbling plumes identified in the southern basin of Fogo

lake (Fig. 11B) coincides with the zone of increased diffuse CO_2 efflux > 2 g m^2 d^{-1} (Fig. 10A) and also with a slight increase in the temperature of the water surface >13ºC (Fig. 10C).

4.4 Subaqueous degasification characteristics of the São Miguel lakes

Several types of hydroacoustic features are identified in the three studied crater lakes that we interpret in terms of sequences reflecting different types of bubbling by subaqueous degasification (Fig. 12). The two main end-members are: (i) the continuous streams of bubbling (flares and clouds) sourced from focused or diffuse sources and (ii) the intermittent bursts of bubbles (crescent shape hyperbolas). Flare-like plumes identified in Furnas are related to continuous streams of bubbles escaping from a focused source (Fig. 12A). The columns identified in the southern basin of Fogo are interpreted as continuous streams of bubbles but sourced diffusely (Fig. 12B). The cloud of bubbles sourced from the deep basin of the Lagoa Azul is interpreted as continuous streams of bubbles but sourced diffusely (Fig. 12C). These types of continuous streams of bubbling coincide with areas where a slight increase in surface temperature is observed as seen in the northern part of Furnas (Fig. 7C), the southern basin of Fogo (Fig. 10C) and the northern deep basin of Lagoa Azul (Fig. 2C). We suggest that these continuous plumes might be formed not only by degassing but alsoby the involvement of hydrothermal waters. Otherwise, intermittent degassing is identified as bursts of bubbles.

The velocity of the rise of bubbles can only be obtained from echograms in Sete Cidades crater lakes. In the case of continuous bubbling, the bubble rising speed can be directly measured by picking the time difference at two distinct depths (yellow and red circles in Fig. 6A) along the same ‘bubble-line’. The different slope of bubble-lines indicates distinct rising speeds (Fig. 6A). The progressive bending of a bubble-line

497 indicates a decrease in rise speeds due to bubble shrinkage (Greinert el al., 2006). The
498 velocities of rise of continuous bubbling in the deep basin of the Lagoa Azul at 23 mwd
499 range from 19 cm/s to 28 cm/s (Fig. 6A). This range of velocities falls within the typical
500 range reported for rising bubbles (20 and 30 cm/s) with sizes between 5 and 20 mm in
501 diameter, respectively (McGinnis et al., 2006). The upwards splitting and deceleration
502 observed in bubble-line echograms (Fig. 6A) is interpreted as the result of breaking up
503 of large bubbles into small ones or the effect of spatial divergence of a few close
504 positioned bubbles that had been released from the bottom nearly simultaneously but
505 could not be distinguished by the acoustic system (multiple targets) as proposed
506 Ostrovsky (2003). When bubbles are not constantly released, the echograms show
507 intermittent bursts of bubbles identified as "crescent shapes" (Figs. 6B, 6C and 6D).
508 The occurrence of bubble bursts at the same water depth allows for the determination of
509 frequencies at which bubbles are released from the lake bottom. From the calculation of
510 the echograms, we observe that the main difference of degassing observed between the
511 Lagoa Azul and Lagoa Verde is the frequency of release of the bubble bursts. The
512 frequency of release in the Lagoa Verde (Fr=31 s) is much slower than the one observed
513 in the Lagoa Azul (Fr=1.0-1.6 s) (Fig. 6). In the other crater lakes Fogo and Furnas, the
514 crescent shape hyperbolas are much more smaller which makes the calculation of
515 bubble release frequency not possible.
516 Echo sounding data revealed a high density of degassing acoustic plumes in the north
517 part of Furnas crater lake (750-900/km^2). In contrast, similar and moderate values of
518 density of bubble plumes are calculated both in the deep basin of the Lagoa Azul
519 (150/km^2) and Lagoa Verde (125-150/km^2), the north and south part respectively of
520 Sete Cidades crater lake and Fogo crater lake (150-200/km^2). The greatest area of lake
521 bottom affected by degassing corresponds to 2.4 km^2 in the northern Lagoa Azul

whereas only 0.9 km^2 is affected in the southern Lagoa Verde. In Fogo crater lake, the extent of the main concentration of bubbling is very reduced (0.158 km^2) and mainly concentrated in their southern basin. The lake bottom area affected by bubble plumes within the Furnas crater lake covers an small extent of 0.1 km^2, mainly concentrated on their northern part around the subaerial hot springs of Caldeira das Furnas.

The meaning of the horizontal acoustic plumes observed in the three crater lakes (Fig. 5C and 5D) is not explained by changes in the geochemical or physical signatures along the vertical profiles (Fig. 3). We suggest that this high backscatter layer could have biological origin related to the level of total dissolution CO_2 at the top of the bubble degasification plumes. In this way, the rising levels of CO_2 sourced from the bubble plumes could be a factor that triggers the intensification of phytoplankton blooms at this level as proposed by Verspagen et al. (2014). The eutrophication of Lake Furnas and Sete Cidades by large blooms of Cyanobacteria and microcystins has been recognized since the 1980s (e.g. Santos et al. 2005). We propose, thus, that the eutrophication acting as a "biological mask" might be the cause for the low CO_2 emission rates measured in the "latent" crater lakes. On the contrary, the observed columns of submarine degassing bubble plumes of CO_2 may trigger phytoplankton blooms at horizontal levels (e.g. Fig. 11B).

4.5. Hydrochemistry of the São Miguel lakes

We used the Cl-SO_4-HCO_3 ternary diagram to classify the Sete Cidades, Furnas and Fogo volcanic lake waters on the basis of the major anion concentrations (Giggenbach, 1991). Figure 13 shows the Cl-SO_4-HCO_3 ternary diagram including the data from Cruz et al. (2006). With the exception of Fogo, similar observations were made by Cruz et al. (2006), the dominant anion in the lake waters was HCO_3^-. Although these waters are

546 located within a crater, they plot in the typical range defined for peripheral waters by
547 Giggenbach, (1991).
548 In Figure 14, we show the $^{3}He/^{4}He$ versus $^{4}He/^{20}Ne$ diagram. The fact that $^{3}He/^{4}He$ and
549 $^{4}He/^{20}Ne$ ratios of the Sete Cidades and Fogo lakes lie on the mixing line between
550 atmospheric and crustal endmembers suggests that dissolved helium is mainly
551 atmospheric with a possible minor addition of crustal (radiogenic) helium. These results
552 indicate negligible mantle helium degassing at these lakes of São Miguel. At Furnas
553 dissolved He showed a slight mantle origin, since it plots close to the air-MORB mixing
554 curve (Fig. 14). The helium emission values are estimated for Furnas Lake (4.2-10.4 mg
555 km^{-2} d^{-1}) and is much lower than those soil diffuse helium emission values reported to
556 date in other volcanic systems: Pico do Fogo, 2.8 x 10^{7} mg km^{-2} d^{-1} (Dionis et al.,
557 2015); Cumbre Vieja volcano, 0.8-1.7 x 10^{5} mg km^{-2} d^{-1} (Padrón et al., 2012) and El
558 Hierro Island, 0.3-1.4 x 10^{5} mg km^{-2} d^{-1} (Padrón et al., 2013). The differences are
559 mainly due to the differences between the diffusion coefficient of helium in water (5.45
560 x 10^{-9} m^{2} s^{-1}) and that for air (7 x 10^{-5} m^{2} s^{-1}). The absence of a clear concentration
561 gradient prevented the theoretical estimation of He emissions using Fick's law in Fogo
562 and Sete Cidades lakes.
563 The highest diffuse CO_2 emission rates coincided spatially with the highest density of
564 bubbles in Furnas volcanic lake. The total CO_2 emissions were estimated from the
565 floating accumulation chamber method, in the range 32-608 kg d^{-1}, represent some of
566 the lowest CO_2 emission rates reported to date for a volcanic lakes (Pérez et al., 2011).
567 In the case of Furnas, the emission value contrasts with the rest of Furnas volcano,
568 which is considered one of the largest CO_2 emitting volcanoes, with a normalizing
569 emission rate of ~186,000 kg km^{-2} d^{-1} (Viveiros et al., 2010). Andrade et al. (2016),
570 reported recently a much higher CO_2 emission rate form the water surface of Furnas

(~321,000 and ~28,000 kg km^{-2} d^{-1} for surveys performed in October-November 2013 and March 2014, respectively). This significant increase does not seem to be caused by the monomictic character of Furnas lake and should be attributed to changes in the volcanic activity of Furnas volcanic system.

These results suggest that observed CO_2 bubble plumes in the three volcanic lakes studied here dissolve almost completely and very rapidly, as has been observed in other volcanic lakes (Caudron et al., 2012). Echo sounding results confirm that most of the subaqueous fumaroles fade out by dissolution of CO_2 before reaching the lake surface. The pH range observed in the three volcanic lakes (~7-9), and almost all total dissolved aqueous CO_2 undergoes ionization in HCO_3^- and CO_3^{2-}. Thus, dissolution processes also minimizes CO_2 molecular diffusion through the water-air interface, reducing greatly the CO_2 emissions towards the atmosphere. Emission rate values, normalized per unit area were very similar for Fogo and Sete Cidades (101-134 kg m^{-2} d^{-1}), and higher than that of Furnas (17 kg m^{-2} d^{-1}). This difference in one magnitude order may be due to the persistent advective discharge of volcano-hydrothermal gases through fumaroles and bubbling pools in Caldeira das Furnas that represent a preferred path for degassing. Since the isotopic composition of CO_2 was not analyzed in this study, a biogenic CO_2 emission cannot be ruled out and prevents to differentiation between a biogenic source and deep degassing.

Even though most of these observed acoustic bubbles are related to only with CO_2 degasification, the occurrence of hydrothermal waters in the vents is cannot be ruled out. Upward migration of water by thermal heating in some areas such as the deep basin of Lagoa Azul, southern Fogo and northern Furnas could explain the relative anomalies of the lake surface temperatures and the type of acoustic features. Therefore, the area with the highest density of bubbling in the Lagoa Azul (Sete Cidades) coincides (Fig.

596 4B) with the positive anomaly of temperature mapped on the lake surface waters (Figs.
597 2C). The northern area of the Furnas crater lake shows spots of anomalous temperatures
598 and relatively low pH close to the subaerial hot-springs of Caldeiras das Furnas (Fig. 7).
599 Furthermore, in this area flares are sourced from carved depressions within the lake
600 bottom suggesting the movement of hydrothermal waters as formation process
601 responsible for these erosional features (Fig. 8).
602 The present degassing at the three crater lakes has a close relationship with recent
603 secondary craters formed around the caldera rim of the three Late Quaternary
604 stratovolcano complexes of São Miguel (e.g. Moore, 1990): i.e. Sete Cidades, Fogo and
605 Furnas. This is indicated by the dense population of acoustic plumes mapped within the
606 lakes, shaped as sub-circular zones. Therefore, the shape of the highest density area of
607 bubble plumes identified at Lagoa Azul and Lagoa Verde is formed in association with
608 ring craters in a roughly circular pattern within the caldera rim of Sete Cidades (Fig.
609 5A). The same occurs in the Furnas crater lake where the main degassing activity is
610 probably associated with a ring crater along the northern rim of the caldera of the
611 Furnas stratovolcano (Fig. 8A).

612 **5. Conclusions**

613 In this work we analyzed the subaqueous degassing from the bottom of three crater
614 lakes by means of a dual beam 50 and 200 kHz echo sounder as part of a
615 multidisciplinary study. Data from the echo sounder has allowed for the detection of a
616 wide range of intensities in the subaqueous degassing that we have classified into two
617 categories: (a) continuous streams to intermittent bursts of bubbles and (b) focused to
618 diffuse sourced degassing. Continuous stream of bubbles released from focused areas of
619 the lake floor were identified as hydroacoustic flare-like shapes having high backscatter
620 signals and rising up to the near surface of the lake. Examples of these focused

621 degassing flares up to 10 m-high have been detected in the northern basin of the Furnas
622 lake close to subaerial hot springs and in the southern basin of Fogo. Continuous
623 degassing but sourced from diffuse areas was identified as “clouds of bubbles”. This
624 type of bubbling was observed mainly from the deep basin of the Lagoa Azul, rising up
625 to 23 m into the water column. The rise speed of the bubble streams averaged 19-28
626 cm/s showing breaking up of large bubbles into small ones and deceleration on their
627 way up from the bottom. Intermittent bursts, types of single/multiple bubbles
628 (“puffing”) were identified as large crescent-like hyperbolas rising into the water
629 column.
630 The frequency of bubble release ranged from 1-2 s in the Lagoa Azul to 31 s in the
631 Lagoa Verde of Sete Cidades lake. The echograms show the bubble(s) ascent at speeds
632 of 30 cm/s near the lake floor diminishing to 15 cm/s at mid-waters and fading by
633 dissolution at c. 2 m below the lake surface. The degassing processes are mainly
634 focused on secondary craters formed near the caldera rims of the three Late Quaternary
635 stratovolcano calderas of São Miguel. Therefore, the highest density of subaqueous
636 fumaroles we have mapped is c. 7.5-9 plumes per 100 m^2 within the northernmost basin
637 of the Furnas caldera rim related to subaerial hot springs. Otherwise, we have measured
638 a moderate density of subaqueous fumaroles as c. 1.5-2 plumes per 100 m^2 within the
639 Fogo lake near the caldera rim of the Agua de Pau stratovolcano and c. 1-1.5 plumes per
640 100 m^2 within the deep basin of the Lagoa Azul lake located near to the caldera rim of
641 the Sete Cidades stratovolcano.
642 Although there is an evident gas discharge from the bottom of the three lakes, observed
643 dissolved CO_2 values indicate that the pressure of this gas in the three lakes remains
644 much lower than the hydrostatic pressure and the risk of limnic eruption is negligible.
645 Otherwise, the acoustic horizontal plumes that appear in the three crater lakes at 1-2 m

beneath the lake surfaces are related to subaqueous fumaroles but cannot be explained by changes in the geochemical or physical signatures along the vertical profiles. This high backscatter acoustic layer could have a biological origin related to CO_2 dissolution of the rising bubbles. Therefore, the CO_2 sourced from dissolution of rising bubbles enhanced by the pH range (~7-9) could be a factor that triggers the intensification of phytoplankton blooms at the subsurface of the lake as proposed by Verspagen et al. (2014). Eutrophication might act as a biological "mask" and thus, might explain the low surface CO_2 degassing measured at the three lakes, in the range 32-608 kg d^{-1}. Following this assumption, the elimination of this biological "mask" may suppose a drastic increase of CO_2 released to the atmosphere from this type of "quiescent" crater lakes (according the classification of Varekamp et al. (2000). Our results emphasize the need to perform regularly surface degassing and hydroacoustic studies as an important volcanic surveillance tool in the Azores archipelago. These studies are of special interest in the case of Furnas due to the recent significant increment in the emission rate of CO_2 reported by Andrade et al. (2016).

Acknowledgements

This work was supported by the following projects: (i) MAKAVOL (MAC/3/C161), co-financed by the European Union Transnational Cooperation Programme MAC 2007–2013; (ii) SUBVENT (CGL2012-39524-C02-02) financed by the R+D+I Spanish National Plan 2008-2011; and (iii) CO2BASAVOL (SolSubC200801000385) financed by the Canary Islands Agency for Research, Innovation and Information Society (ACIISI) of the Government of the Canary Islands, as well as the Observatório Vulcanológico e Geotérmico dos Açores (OVGA) and the Cabildo Insular de Tenerife. The authors are grateful to Helen Robinson for help with English.

References

671 ANDRADE, C, VIVEIROS, F., CRUZ, J.V., COUTINHO, R. & SILVA, C. 2016. Estimation of
672 the CO_2 flux from Furnas volcanic Lake (São Miguel, Azores). *Journal of*
673 *Volcanology and Geothermal Research*, **315**, 51–64.
674 BOOTH, B., CROASDALE, R. & WALKER, G.P.L. 1978. A quantitative study of five
675 thousand years of volcanism on São Miguel, Azores. *Royal Society of London*
676 *Philosophical Transactions*, **288**, 271-319.
677 CAPASSO, G. & INGUAGGIATO, S. 1998. A simple method for the determination of
678 dissolved gases in natural waters. An application to thermal waters from Vulcano
679 Island. *Applied Geochemistry,* **13** (5), 631-642.
680 CARDELLINI, C., CHIODINI, G. & FRONDINI, F. 2003. Application of stochastic simulation
681 to CO_2 flux from soil: mapping and quantification of gas release. *Journal of*
682 *Geophysical Research: Solid Earth*, **108** (B9), 2425, doi:10.1029/2002JB002165.
683 CAUDRON, C., MAZOT, A. & BERNARD, A. 2012. Carbon dioxide dynamics in Kelud
684 volcanic lake. *Journal of Geophysical Research: Solid Earth*, **117** (B5), doi:
685 10.1029/2011JB008806.
686 CLARKE, W.B., JENKINS, W.B. & TOP, Z. 1976. Determination of tritium by mass
687 spectrometric measurement of ^3He. *The International Journal of Applied*
688 *Radiation and Isotopes*, **27**, 515–522, doi:10.1016/0020-708X(76)90082-X.
689 COLE, J.J., CARACO, N.F., KLING, G.W. & KRATZ, T.K. 1994. Carbon dioxide
690 supersaturation in the surface waters of lakes. *Science*, **265**, 1568–1570.
691 CRUZ, J.V., COUTINHO, R.M., CARVALHO, M.R., OSKARSSON, N. & GISLASON, S.R.
692 1999. Chemistry of waters from Furnas volcano, São Miguel, Azores: fluxes of
693 volcanic carbon dioxide and leached material. *Journal of Volcanology and*
694 *Geothermal Research,* **92**, 151–167.

695 CRUZ, J.V., ANTUNES, P., AMARAL, C., FRANÇA, Z. & NUNES, J.C. 2006. Volcanic lakes
696 of the Azores archipelago (Portugal): Geological setting and geochemical
697 characterization. *Journal of Volcanology and Geothermal Research,* **156**, 135–
698 157.
699 CRUZ, J.V. & FRANÇA, Z. 2006. Hydrogeochemistry of thermal and mineral water
700 springs of the Azores archipelago (Portugal). *Journal of Volcanology and*
701 *Geothermal Research*, **151**, 382–398.
702 DEUTSCH, C. & JOURNEL, A. 1998. *GSLIB: Geostatistical Software Library and User's*
703 *Guide*. Oxford University Press, New York.
704 DIONIS, S., MELIÁN, G., RODRÍGUEZ, F., HERNÁNDEZ, P., PADRÓN, E., PÉREZ, N.,
705 BARRANCOS, J., PADILLA, G., SUMINO, H., FERNANDES, P., BANDOMO, Z., SILVA,
706 S., PEREIRA, J. & SEMEDO, H. 2015. Diffuse volcanic gas emission and thermal
707 energy release from the summit crater of Pico do Fogo, Cape Verde. *Bulletin of*
708 *Volcanology*, **77**, 1–13, doi:10.1007/s00445-014-0897-4.
709 FORJAZ, V.H. 1984. São Miguel volcanostratigraphic sketch. Geosciences Department,
710 University of the Azores, Ponta Delgada, in Portuguese.
711 GIGGENBACH, W.F. 1991. Chemical techniques in geothermal exploration. *In:*
712 D'AMORE, F. (ed) *Application of geochemistry in geothermal reservoir*
713 *development*. UNITAR/UNDP publication, Rome, 119-142.
714 GRAHAM, D.W. 2002. Noble gas isotope geochemistry of Mid-Ocean Ridge and Ocean
715 Island Basalts: characterization of mantle source reservoirs. *In*: PORCELLI,
716 D.,BALLENTINE, C.J., WIELER, R. (eds) *Noble Gases in Geochemistry and*
717 *Cosmochemistry*. *Reviews in Mineralogy and Geochemistry* **47**, 247–317.
718 GREINERT, J., ARTEMOV, Y., EGOROV, V., DE BATIST, M. & MCGINNIS, D. 2006. 1300-
719 m-high rising bubbles from mud volcanoes at 2080 m in the Black Sea:

720 Hydroacoustic characteristics and temporal variability. *Earth and Planetary*
721 *Science Letters*, **244**, 1–15, doi:10.1016/j.epsl.2006.02.011.
722 GREINERT, J., MCGINNIS, D.F., NAUDTS, L., LINKE, P. & DE BATIST, M. 2010.
723 Atmospheric methane flux from bubbling seeps: Spatially extrapolated
724 quantification from a Black Sea shelf area. *Journal of Geophysical Research*, **115**,
725 C01002, doi:10.1029/2009JC005381.
726 HUTTUNEN, J.T., ALM, J., LIIKANEN, A., JUUTINEN, S., LARMOLA, T., HAMMAR, T.,
727 SILVOLA, J. &. MARTIKAINEN P.J. 2003. Fluxes of methane, carbon dioxide and
728 nitrous oxide in boreal lakes and potential anthropogenic effects on the aquatic
729 greenhouse gas emissions. *Chemosphere*, **52**(3), 609-621.
730 KLING, G.W., EVANS, W.C., TANYILEKE, G., KUSAKABE, M., OHBA, T., YOSHIDA, Y. &
731 HELL, J.V. 2005. Degassing Lakes Nyos and Monoun: Defusing certain disaster.
732 *Proceedings of the National Academy of Sciences*, **102**, 14185–14190, doi:
733 10.1073/pnas.0502274102.
734 KUSAKABE, M., TANYILEKE, G.Z., MCCORD, S.A. & SCHLADOW, S.G. 2008. Evolution
735 of CO_2 in Lakes Monoun and Nyos, Cameroon, before and during controlled
736 degassing. *Geochemical Journal*, **42**, 93–118.
737 LE GUERN, F. & SIGVALDASON, G.E. 1989. The Lake Nyos event and natural CO_2
738 degassing I. *Journal of Volcanology and Geothermal Research*, **39**, 95–275.
739 LOURENÇO, N., MIRANDA, J.M., LUIS, J.F., RIBEIRO, A., MENDES VICTOR, L.A.,
740 MADEIRA, J. & NEEDHAM, H.D. 1998. Morpho-tectonic analysis of the Azores
741 volcanic plateau from a new bathymetric compilation of the area. *Marine*
742 *Geophysical Research*, **20**, 141-156.
743 MCGINNIS, D. F., GREINERT, J., ARTEMOV, Y., BEAUBIEN, S.E. & WÜEST, A. 2006. Fate
744 of rising methane bubbles in stratified waters: How much methane reaches the

745 atmosphere?. *Journal of Geophysical Research*, **111**, C09007,
746 doi:10.1029/2005JC003183.
747 MIRANDA, J.M., LUIS, J.F., LOURENÇO, N. & GOSLIN, J. 2014. Distributed deformation
748 close to the Azores Triple "Point". *Marine Geology,* **355**, 27-35.
749 MOORE, R.B. 1990. Volcanic geology and eruption frequency, São Miguel, Azores.
750 *Bulletin of Volcanology,* **52**, 602-514.
751 MOORE, R.B. 1991. Geology of the three quaternary stratovolcanoes on São Miguel,
752 Azores. *U.S. Geological Survey Bulletin*, **1900**, 46 pp.
753 MORGAN, L.A., SHANKS III, W.C., LOVALVO, D.A, JOHNSON, S.Y., STEPHENSON, W.J.,
754 PIERCE, K.L., HARLAN, S.S, FINN, C.A., LEE, G., WEBRING, M., SCHULZE, B.,
755 DÜHN, J., SWEENEY, R. & BALISTRIERI, L. 2003. Exploration and discovery in
756 Yellowstone Lake: Results from high-resolution sonar imaging, seismic reflection
757 profiling and submersible studies. *Journal of Volcanology and Geothermal*
758 *Research*, **122**, 221–242, doi:10.1016/S0377-0273(02)00503-6.
759 PADRÓN, E., PÉREZ, N.M., HERNÁNDEZ, P.A., SUMINO, H., MELIÁN, G., BARRANCOS, J.,
760 NOLASCO, D., PADILLA, G., DIONIS, S., RODRÍGUEZ, F., HERNÁNDEZ, I., CALVO,
761 D., PERAZA, M.D. & NAGAO, K. 2013. Diffusive helium emissions as a precursory
762 sign of volcanic unrest. *Geology,* **41**(5), 539-542, doi:10.1130/G34027.1.
763 PADRÓN, E., PÉREZ, N.M., HERNÁNDEZ, P.A., SUMINO, H., MELIÁN, G., BARRANCOS, J.,
764 NOLASCO, D. & PADILLA, G. 2012. Helium emission at Cumbre Vieja volcano, La
765 Palma, Canary Islands. *Chemical Geology*, **312-313**, 138–147.
766 doi:10.1016/j.chemgeo.2012.04.018.
767 PARKINSON, K. J. 1981. An improved method for measuring soil respiration in the field.
768 *Journal of Applied Ecology*, **18**, 221-228.

769 PÉREZ, N.M., HERNÁNDEZ, P.A, PADILLA, G., NOLASCO, D., BARRANCOS, J., MELÍAN,
770 G., PADRÓN, E, DIONIS, S., CALVO, D., RODRÍGUEZ, F., NOTSU, K., MORI, T.,
771 KUSAKABE, M., ARPA, M.C., RENIVA, P. & IBARRA, M. 2011. Global CO_2
772 emission from volcanic lakes. *Geology*, **39,** 235-238.
773 QUEIROZ, G. & GASPAR, J.L. 1998. The geology of Sete Cidades volcano, S. Miguel
774 island, Azores. *EC Advanced Study Course, volcanism hazard assessment,*
775 *monitoring and risk mitigation*, Ponta Delgada, São Miguel, 46p.
776 SANTOS, M.C.R., MEDEIROS PACHECO D.M., SANTANA F. & MUELLE, H. 2005.
777 Cyanobacteria blooms in Sete-Cidades lake (S. Miguel Island - Azores).
778 Algological Studies 117 (Cyanobacterial Research 6): 393- 406.
779 SIGURDSSON, H., DEVINE, J.D., TCHOUA, F.M., PRESSER, T.S., PRINGLE, M.K.W. &
780 EVANS, W.C. 1987. Origin of the lethal gas burst from Lake Monoun, Cameroun.
781 *Journal of Volcanology and Geothermal Research*, **31**, 1–16, doi: 10.1016/0377-
782 0273(87)90002-3.
783 SHOTTON, F.W. & WILLIAMS, R.E.G. 1971. Birmingham University radiocarbon dates,
784 V. *Radiocarbon*, **13**, 141-156.
785 SUMINO, H., NAGAO, K. & NOTSU, K. 2001. Highly sensitive and precise measurement
786 of helium isotopes using a mass spectrometer with double collector system.
787 *Journal of the Mass Spectrometry Society of Japan*, **49**, 61-68.
788 TAKANO, B., SAITOH, H. & TAKANO, E. 1994. Geochemical implications of subaqueous
789 molten sulfur at Yugama crater lake, Kusatsu-Shirane volcano, Japan.
790 *Geochemical Journal*, **28**, 199-216.
791 TROTA, A.N. 1998. Main alignments in São Miguel island obtained from aerial photo-
792 interpretation. *EC. Advanced Study Course, volcanism hazard assessment,*
793 *monitoring and risk mitigation*. Ponta Delgada, São Miguel, 91p.

794 VAREKAMP, J.C., PASTERNACK, G.B. & ROWE JR., G.L. 2000. Volcanic lake systematics
795 II. Chemical constraints. *Journal of Volcanology and Geothermal Research* **97**,
796 161–179.
797 VERHALLEN, P.T.H.M., OOMEN, L.J.P., ELSEN, A.J.J.M., & KRUGER, A.J. 1984. The
798 diffusion coefficients of helium, hydrogen, oxygen and nitrogen in water from the
799 permeability of a stagnant liquid layer in the quasi-steady state. *Chemical*
800 *Engineering Science*, **39**, 1535-1541.
801 VERSPAGEN J.M.H., VAN DE WAAL D.B., FINKE J.F., VISSER P.M., VAN DONK, E. &
802 HUISMAN, J. 2014. Rising CO_2 Levels Will Intensify Phytoplankton Blooms in
803 Eutrophic and Hypertrophic Lakes. PLoS ONE 9(8): e104325.
804 doi:10.1371/journal.pone.0104325
805 VIVEIROS, F., CARDELLINI, C., FERREIRA, T., CALIRO, S., CHIODINI, G. & SILVA, C. 2010.
806 Soil CO_2 emissions at Furnas volcano, São Miguel Island, Azores archipelago:
807 Volcano monitoring perspectives, geomorphologic studies, and land use planning
808 application. *Journal of Geophysical Research: Solid Earth*, **115**(B12), doi:
809 10.1029/2010JB007555.
810 WALLENSTEIN, N., DUNCAN, A., CHESTER, D. & MARQUES, R. 2007. Fogo Volcano (São
811 Miguel, Azores): a hazardous edifice. *Géomorphologie: relief, processus,*
812 *environnement*, **3/2007**, url: http://geomorphologie.revues.org/2853.
813 DOI:10.4000/geomorphologie.2853.
814 WESTON, F.S. 1964. List of recorded volcanic eruptions in the Azores with brief reports.
815 *Boletim do Museu e Laboratorio Mineralogico e Geologico da Faculdade de*
816 *Ciencias*, **10**, 3-18.

ZBYSZEWSKI, G., DE MEDEIROS, A.C., DE ALMEIDA, F.M. & DA VEIGA FERREIRA, O. 1958. Carta geologica de Portugal na escala de 1:50,000 (São Miguel): Servicos Geologicos de Portugal, Lisbon.

Figure captions:

Figure 1. Map of São Miguel Island, Azores showing the location of Sete Cidades, Fogo and Furnas volcanic lakes.

Figure 2. Spatial distribution of surface CO_2 emission (A), water pH (B) and water temperature (C) values at Sete Cidades volcanic lake. Solid black dots and white star indicate sampling sites and vertical profiles locations, respectively.

Figure 3. Results of the physico-chemical parameters analyzed at different depths along vertical profiles in Sete Cidades (A-E), Furnas (G-L) and Fogo (M-R) volcanic lakes. F: Variation of total dissolved CO_2 with depth in Sete Cidades, Furnas and Fogo volcanic lakes, São Miguel. Symbols: Lagoa Azul: closed squares, Lagoa Verde: open squares, N-profile Furnas: closed circles, S-profile Furnas: open circles and Fogo: open triangles

Figure 4. 3D bathymetric image of the Sete Cidades crater lake (A), Lagoa Azul (B) and Lagoa Verde (C). Red dots show the location of bubble plumes.

Figure 5. Location (A) and density map (B) of bubble plumes within the Sete Cidades crater lake. Echograms (50 kHz) of the Lagoa Azul (C) and Lagoa Verde (D) portraying well defined bubble plumes rising from the bottom of the lake, h= acoustic hyperbola. Color scale in C and D: green to yellow color reflects high concentration of bubbles (high scattering) and blue for low concentration (low scattering).

Figure 6. (A) Echogram (50 kHz) used to calculate the speed of the rising bubbles according the depth-time for each `bubble line´ in the Lagoa Azul crater lake. The red

840 and yellow dots indicate that bubbles rise at 19 and 28 cm/s respectively. (B) and (C)
841 show echograms (50 kHz) illustrating the intermittency of the degassing process
842 `puffing´ in the Lagoa Azul crater lake. Bursts of bubbles are emitted every 1-2 s. (D)
843 and (E) show echograms (50 kHz) and interpretation respectively used to calculate the
844 speed of rise of bubbles and the frequency of intermittent bubbling in the Lagoa Verde.
845 Bursts of bubbles rise at velocities of 30 cm/s close to the bottom reducing their velocity
846 to 15 cm/s as they ascend. The reduction in the rise velocities is related to the
847 diminution of the bubble diameters as they dissipate. Bubble plumes disappear though
848 the water column due to fast dissolution. Frequency of bubble bursts is obtained by
849 calculating the time between two bubbles at the same water depth. In this case, the
850 frequency between bubble bursts is 31 s. See text for further explanation.

851 **Figure 7.** Spatial distribution of surface CO_2 emission (A), water pH (B) and
852 temperature (C) values at Furnas volcanic lake. Solid black dots and star (white: N-
853 profile and pink: S-profile) indicate sampling sites and vertical profile locations,
854 respectively.

855 **Figure 8.** (A) Location of bubble plumes within the Furnas crater lake. (B) Echogram
856 (50 kHz) showing well-defined acoustic flares at the north side of the Furnas crater lake.
857 Some plumes are rooted on depressions (`furnas´) at the bottom of the lake.

858 **Figure 9.** (A) Density maps of bubble plumes in the north of Furnas crater lake. (B) 3D
859 image of the flares rising from the bottom of the Furnas crater lake.

860 **Figure 10.** Spatial distribution of surface CO_2 emission (A), water pH (B) and
861 temperature (C) values at Fogo volcanic lake. Solid black dots and white star indicate
862 sampling sites and vertical profile locations, respectively.

Figure 11. (A). Location of bubble plumes and bathymetry of the Fogo crater lake. (B). Echogram (50 kHz) showing well-defined vertical bubble plumes linked by a horizontal plume beneath the surface of the lake in the southern basin of the Fogo crater lake. (C) Density maps of bubble plumes in the Fogo crater lake.

Figure 12. The sequence of acoustic features and their relationship with degassing processes in the studied crater lakes. The end-members are continuous vs. intermittent degassing and focused vs. diffused sources. Further explanation in the text.

Figure 13. Classification of waters from Sete Cidades, Furnas and Fogo volcanic lakes on the basis of relative Cl^-, SO_4^{2-} and HCO_3^- content (in mg/L). Data from Cruz et al. (2006) are displayed as solid black symbols.

Figure 14. $^3He/^4He$ vs. $^4He/^{20}Ne$ diagram for dissolved gas from the bottom of Lagoa Azul, Lagoa Verde, Furnas (N- and S-profile) and Fogo crater lakes. Grey curves indicate calculated binary mixing lines between air saturated water (ASW), crustal ($^3He/^4He$ = 0.01 R_A) and mantle ($^3He/^4He$ = 8 ± 1 R_A, Graham, 2002) endmember compositions, having an assumed $^4He/^{20}Ne$ ratio of 10^6 and 10^3 respectively.

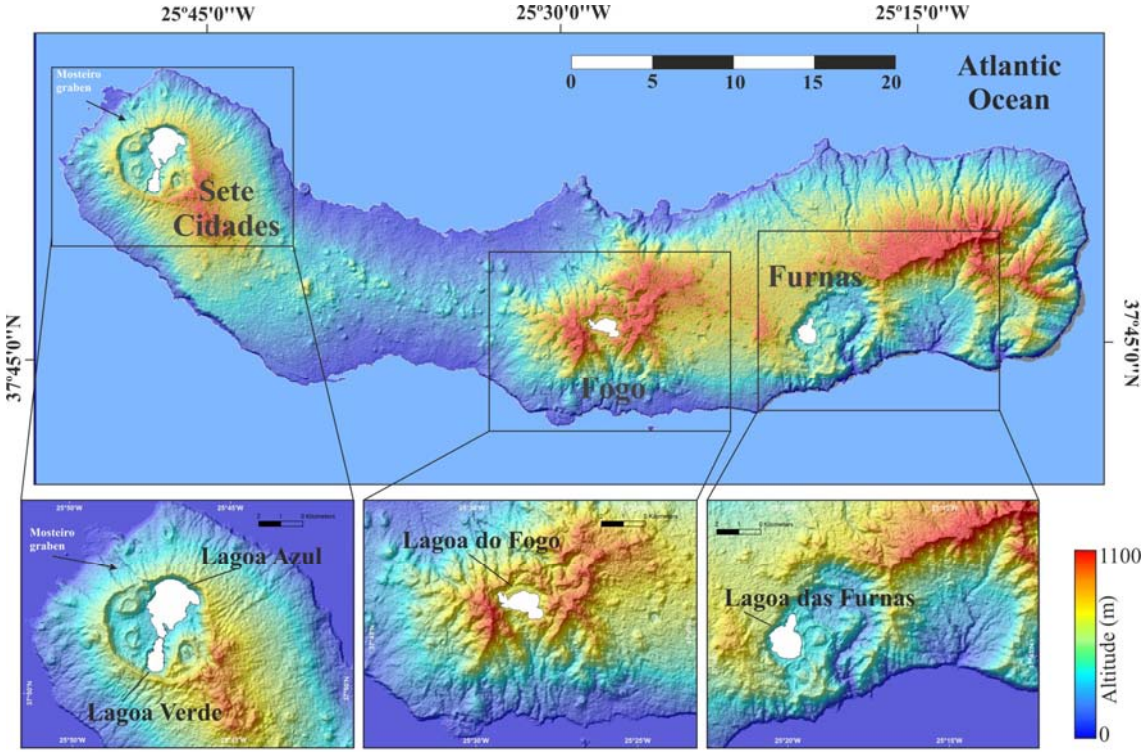

879

880 Fig.1

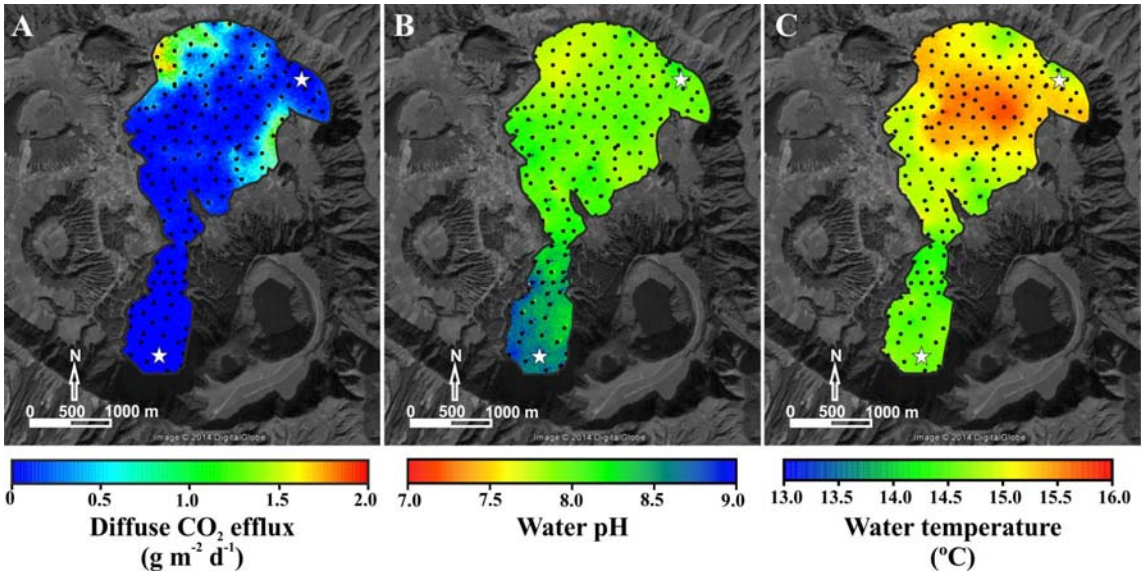

881

882 Fig.2

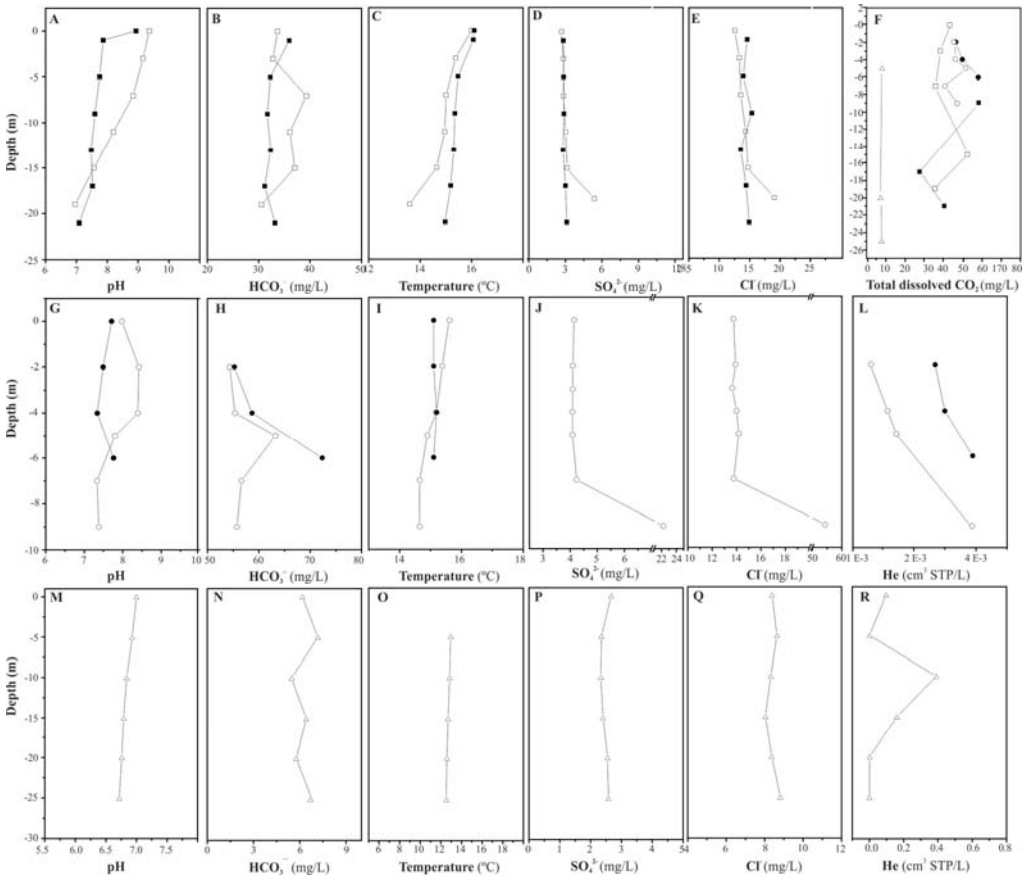

883

884 Fig.3

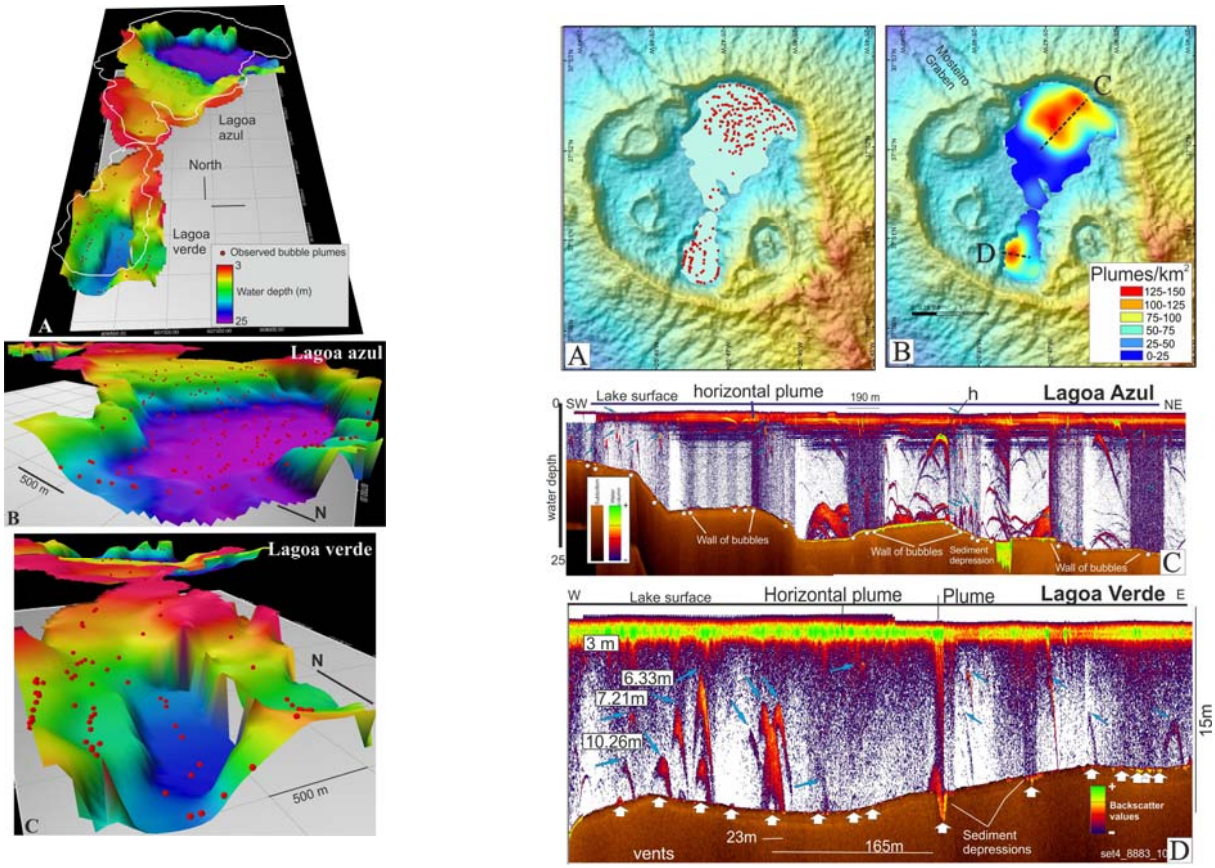

885

886 Fig.4 Fig.5

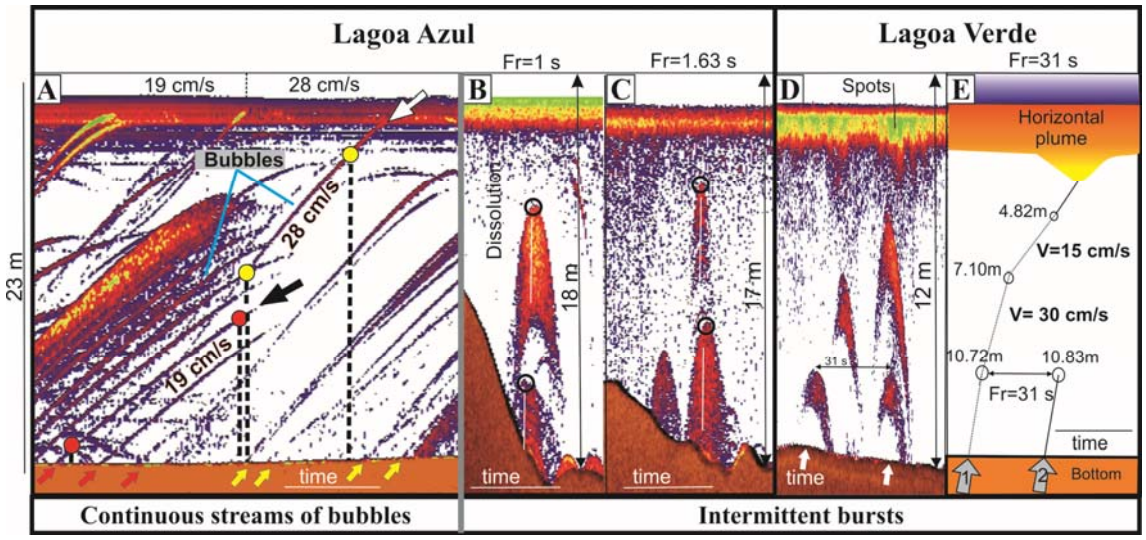

887

888 Fig.6

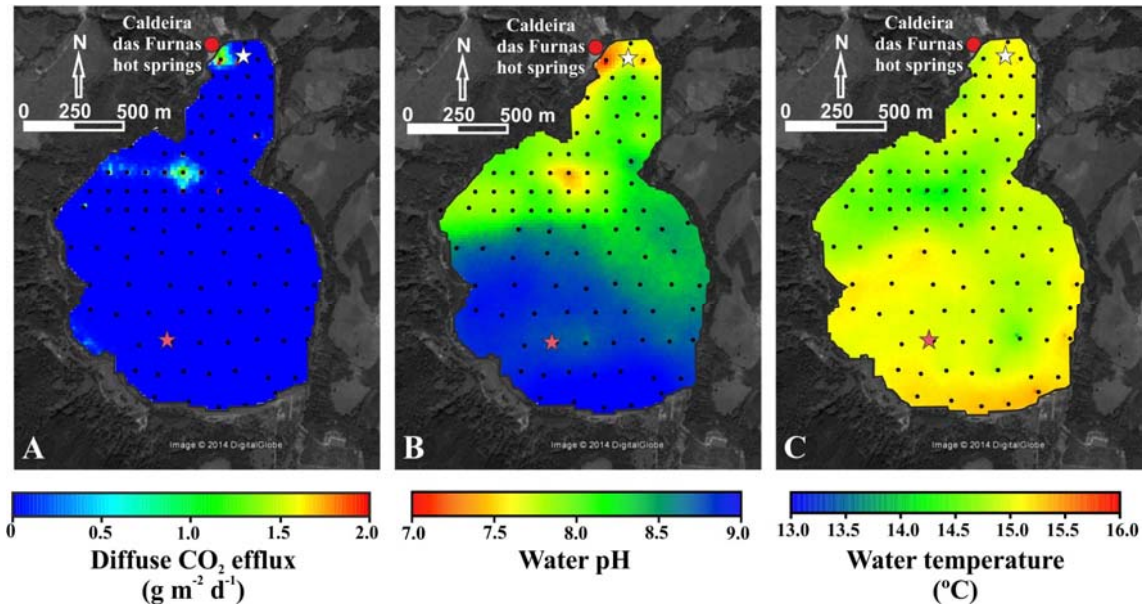

889

890 Fig.7

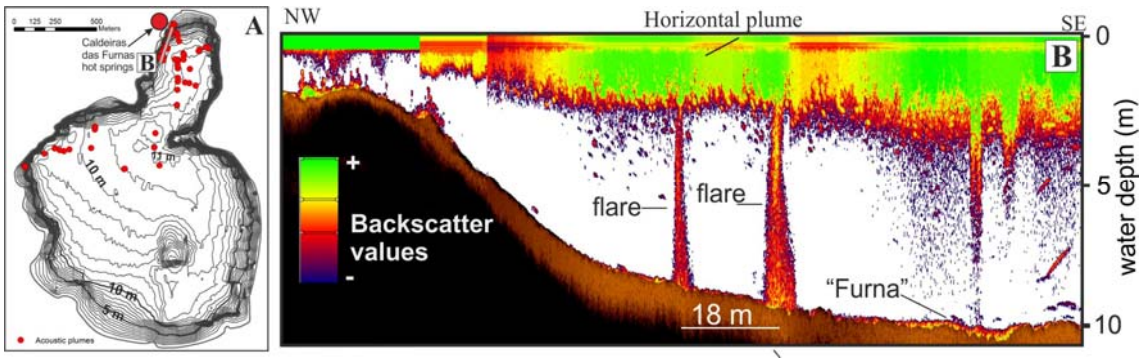

891

892 Fig.8

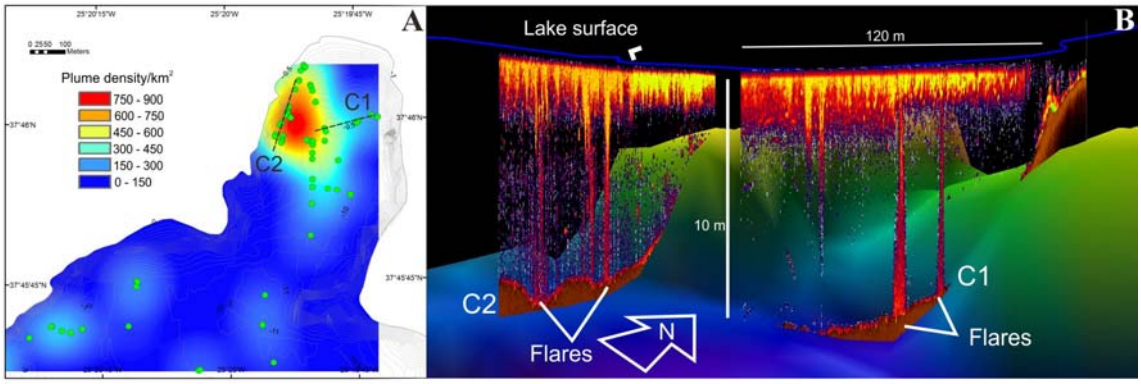

Fig.9

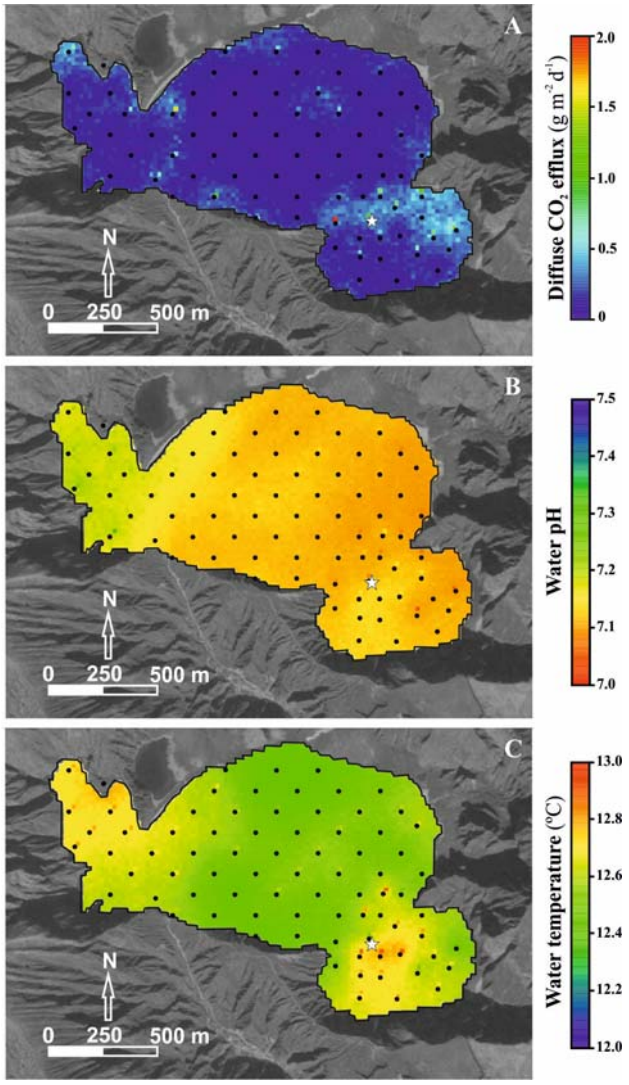

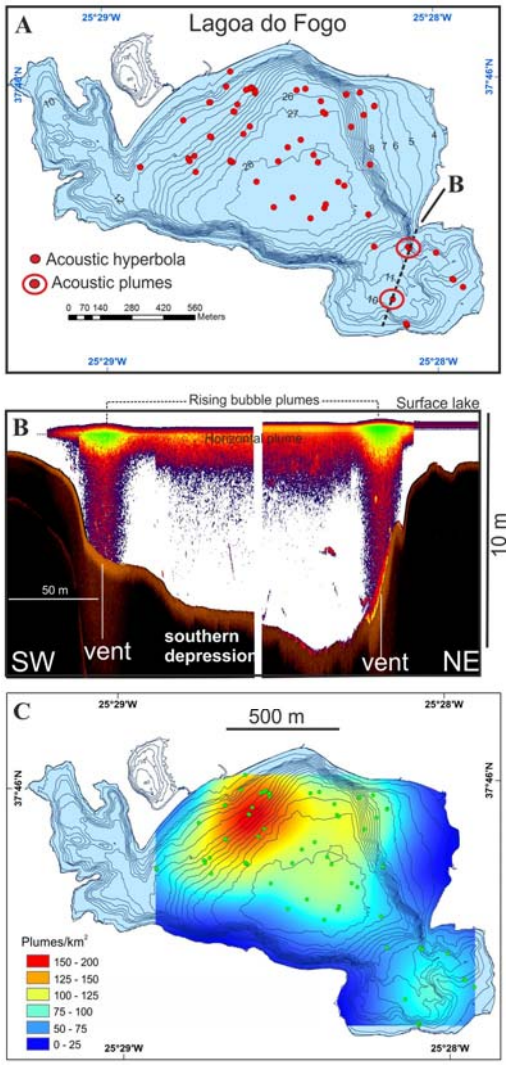

Fig.10

Fig.11

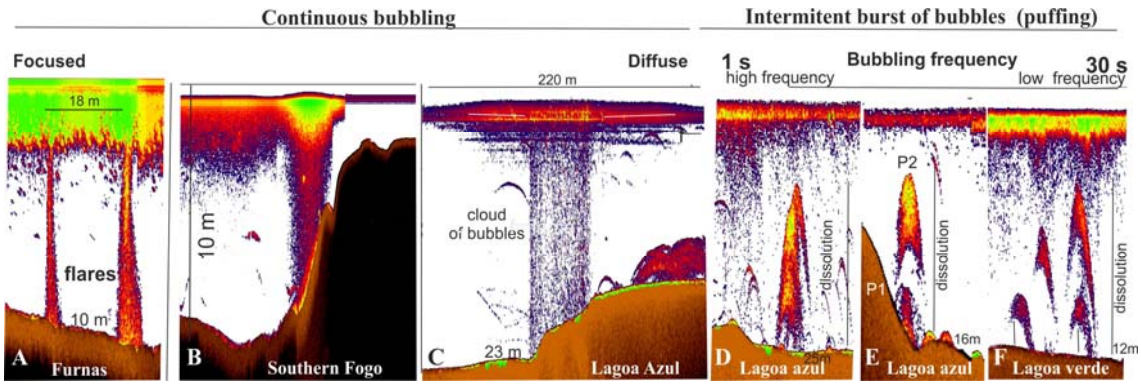

900

901 Fig.12

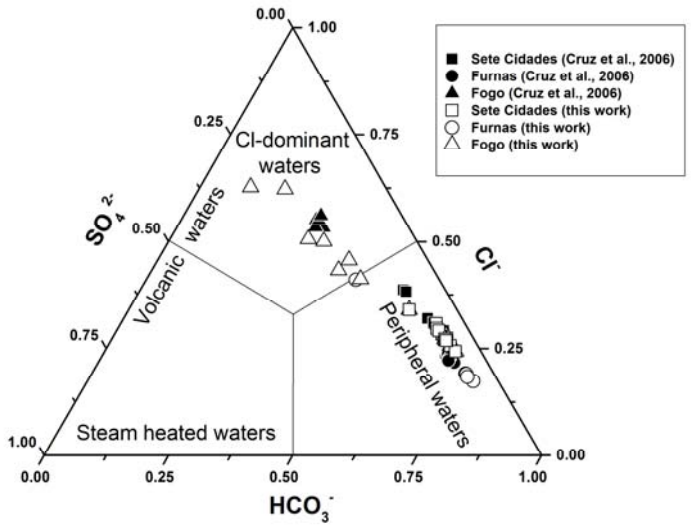

902

903 Fig.13

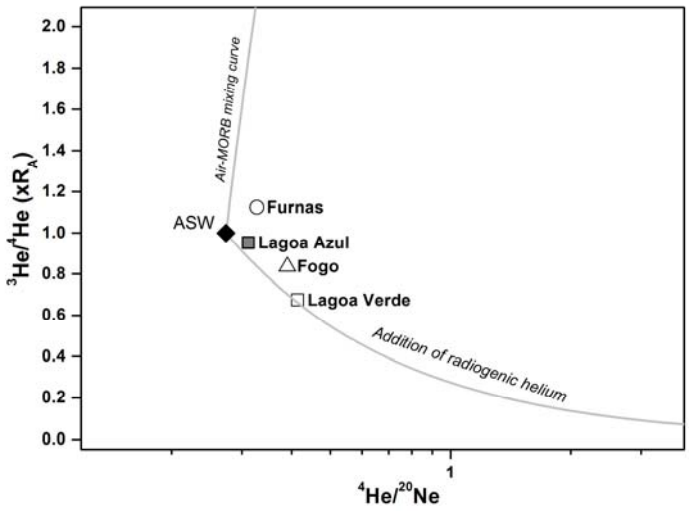

904

905 Fig.14